

## **Crustal Thickness along the Traverse from Zhongshan to Dome A in East Antarctica**

FENG Mei<sup>1,\*</sup>; AN Meijian<sup>1</sup>; AN Chunlei<sup>2</sup>; SHI Guitao<sup>2</sup>; ZHAO Yue<sup>1</sup>; LI Yuansheng<sup>2</sup>;

Douglas Wiens<sup>3</sup>

<sup>1</sup>Institute of Geomechanics, Chinese Academy of Geological Sciences, Beijing 100081, China;

<sup>2</sup>Polar Research Institute of China, Shanghai 200136, China;

<sup>3</sup>Dept. of Earth and Planetary Sci., Washington University, St. Louis, MO 63130-4899, USA

### **Abstract**

From the 4th International Polar Year (IPY) in 2007/08 through 2013, Chinese have deployed cold-mode very broadband seismic stations along the Chinese Antarctic Research Expedition traverse from Zhongshan to Kunlun at Dome A, East Antarctica. We retrieved S-receiver functions from seismic waveform observations at seven of the stations, and inverted these data to obtain the crustal thickness beneath each station. The results show that along the traverse, the crustal thickness of 38 km beneath Zhongshan station increases to ~58 km beneath stations EAGLE and CHNB, decreases to 47 km beneath station CHNA, and increases to 62 km beneath Dome A, the highest point on Antarctica. Crustal thickness variations correlate with bedrock surface variations along the traverse, indicating that the tectonic regime between Zhongshan and station CHNB is relatively homogeneous. The crustal thickness beneath Dome A, which is the largest known crustal thickness in Antarctica, is substantially greater than that beneath the cratons of other continents. The crustal thickness beneath station CHNA is ~10 km less than that beneath neighbouring stations; however, this difference may be the result of the relatively short duration of observations at station CHNA, or may indicate large lateral variations in crustal structure beneath the Gamburtsev Subglacial Mountains.

**Keywords:** crustal thickness, seismic station, Dome A, East Antarctica, Antarctic expedition

---

\*Corresponding author (email: [mei\\_feng\\_cn@163.com](mailto:mei_feng_cn@163.com))

## 1. Introduction

During the Mesozoic breakup of the Gondwana supercontinent, East Antarctica separated from the African, Indian, and Australian continents. Research on the continental crust of Antarctica can contribute to an understanding of the processes and dynamics involved in the formation and break-up of Gondwana. However, more than 90% of Antarctica is covered with several kilometres of ice ([Fretwell et al., 2013](#)), and efforts to unravel the geologic history of the continent have been hindered by a combination of limited access to rock outcrops on account of ice cover and logistical limitations to the collection of geophysical data. Prior to 2007, because of the region's harsh environmental conditions, no seismological research or exploration had been conducted in the region of the Gamburtsev Subglacial Mountains (GSM) or nearby areas of East Antarctica (EANT). Consequently, studies on the crust of East Antarctica have important implications for the understanding of geophysical processes on the continent.

Since the 4th International Polar Year (IPY) in 2007/08, and as part of the Gamburtsev Antarctic Mountains Seismic Experiment (GAMSEIS) component of the Antarctica's Gamburtsev Province (AGAP) IPY project (2007–2010), international communities deployed tens of cold-mode very broadband seismic stations in the GSM and peripheral areas ([Hansen et al., 2010](#)). As part of the international GAMSEIS project and under the management of the Chinese Program of Antarctic Nova Disciplines Aspects (PANDA), China has deployed eight seismic stations along the CHINARE traverse between Chinese Zhongshan and Kunlun, Dome A, between 2007/08 and 2013 (see Figure 1). The seismic data from the stations are suitable for the study of deep crustal structures.

The Moho discontinuity, the interface between crust and mantle, was identified by Mohorovičić ([1910](#)) one century ago. Crustal thickness, the distance from the Earth's surface to the Moho, is related to regional tectonic history and geodynamic environment. A number of studies were conducted to investigate the crustal thickness along parts of Antarctica's continental margin prior to the 4<sup>th</sup> IPY ([Baranov and Morelli, 2013](#) and references therein). In all methods measuring crustal thickness, analysing receiver functions at seismic stations ([Langston, 1979](#)) is one of simplest methods involves measurements to the depth of the Moho and has been applied to measurements of crustal thickness in Antarctica ([Winberry and](#)

[Anandakrishnan, 2004](#); [Bayer et al., 2009](#)). The data recorded at GAMSEIS stations allows for measurements of crustal thickness beneath most of the GAMSEIS stations by receiver function analyses ([Hansen et al., 2009](#); [2010](#)).

All crustal thicknesses obtained prior to the present study are indicated in Figure 1. Notably, no data are available for crustal thickness beneath the Chinese stations from Zhongshan to Dome A, including for the stations in the area of the Lambert rift. The whole EANT is a craton and stable for hundreds of million years ([An et al., 2013](#)), and the Lambert rift was the largest active tectonic area on the Antarctic continent during the late Palaeozoic ([Harrowfield et al., 2005](#); [Phillips and Läufer, 2009](#)). Therefore, the study of the crust beneath the Chinese stations may contribute to an understanding of the regional tectonic evolution of the GSM and the Lambert rift. In this study, we report on the retrieval of crustal thickness data beneath the Chinese stations using the method of receiver function analysis.

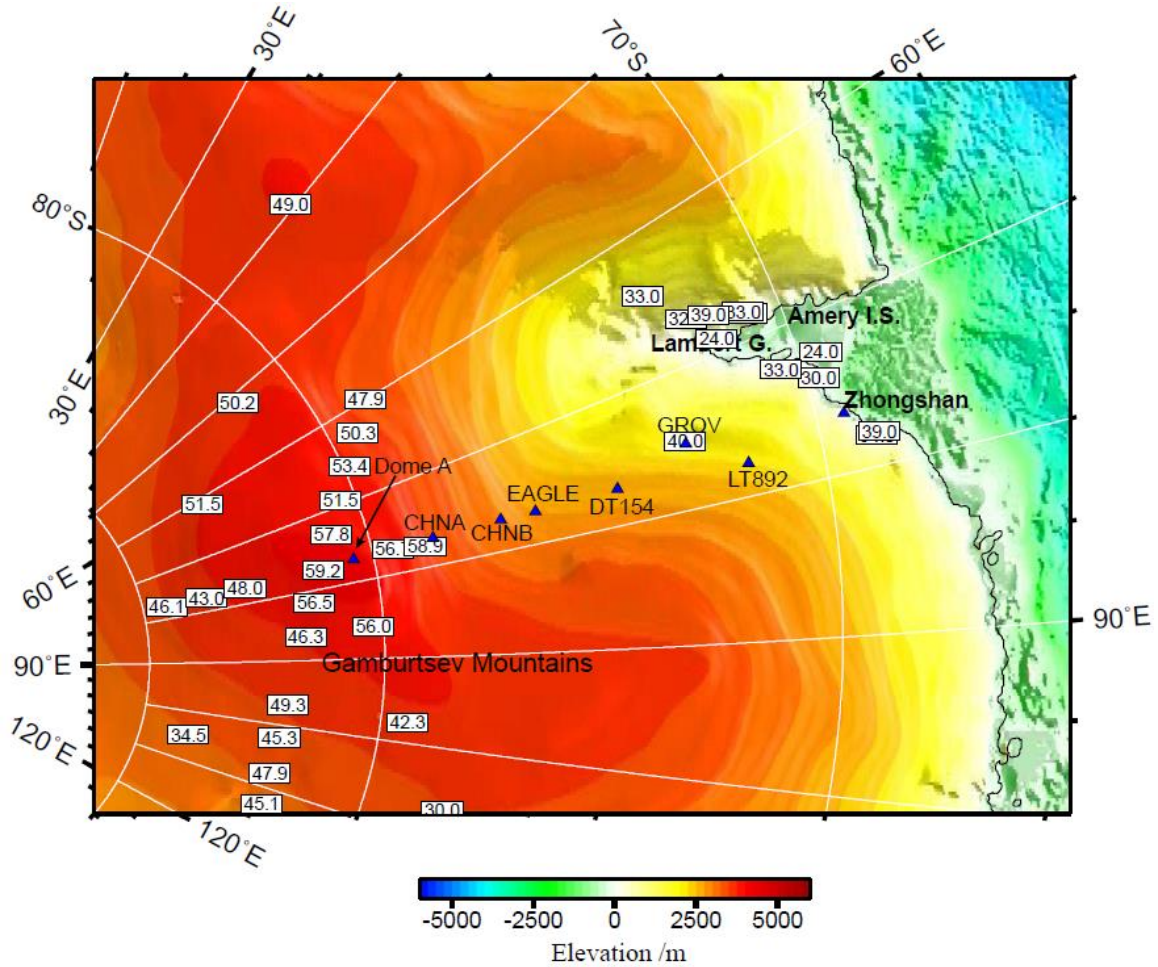


Figure 1. Elevation map of East Antarctica showing the locations of Chinese seismic stations (blue triangles) and Moho depths (numerical labels, in kilometres; data from An et al. (2013)).

## 2. Data and processing

### 2.1 Data

We retrieved S-wave receiver functions (SRFs) from the waveform data recorded at the Chinese stations from Zhongshan to Dome A, and used the SRFs to obtain the crustal thickness beneath each station. We collected data from all eight cold-mode very broadband stations (Figure 1) during the period from the 4<sup>th</sup> IPY (2007/08) to early 2013. The operation times at each station, shown in Figure 2, were such that only a small amount of valid data (as little as one month) was obtained at a given station. The short duration of observations at Zhongshan (station ZHSH) was due to its recent installation date (late 2012). Station GROV has not been revisited by the Chinese expedition team since its installation.

All stations, except for station ZHSH, are installed on ice. The seismic station at Dome A (called DOMEA) and nearby stations are located in areas for which conditions for observation are relatively poor (e.g., long transport distances, long polar nights, and extremely low temperatures). Solar panels are the only power supply at the seismic stations, and therefore the stations do not operate during the long polar night. Only a small amount of valid data were collected at most stations, especially at stations ZHSH, LT892, and GROV. However, while the amount of valid data is limited, the data are still enough to provide reliable information on crustal thickness that was previously unavailable prior to the installation of the Chinese seismic station network. Because the number of earthquake events recorded by station GROV is insufficient to give a reliable result, we will not analyse or discuss the data from this station, but will limit our discussion to receiver function analyses from the other seven stations.

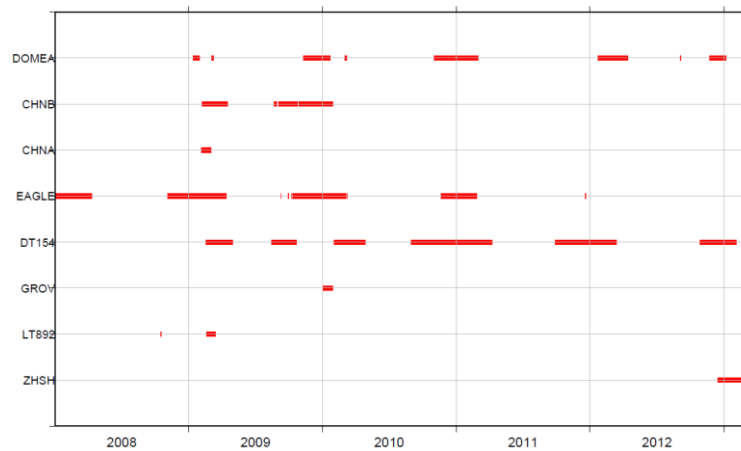


Figure 2. Gantt chart, with red bars showing the times during which valid data were obtained at a given station. ZHSH = Zhongshan, DOMEA = Dome A (Kunlun). The locations of the stations are shown in Figure 1.

## 2.2 S-wave receiver functions

A receiver function, which is a type of waveform extracted from a three-component seismic waveform, reflects the Earth's structure just beneath the receiver ([Langston, 1979](#)). P-wave receiver functions are commonly used to determine crustal thickness. However, all of the seismic stations deployed in inland Antarctica are installed on ice with a thickness of 1–3

km ([Fretwell et al., 2013](#)), and the multiple waves caused by the ice layer overlap with the Pms and Ps waves that are converted from direct P waves, which greatly reduces the reliability of crustal thicknesses determined from P-wave receiver functions. On the other hand, Smp and Sp waves converted from S-wave receiver functions can be easily discriminated, because the converted waves arrive earlier than the S-wave, whereas the multiple waves resulting from the ice layer arrive later than the S-wave ([Hansen et al., 2009](#)). Hence, S-wave receiver functions are more useful than P-wave receiver functions for determinations of crustal thickness in the circumstances encountered along the CHINARE traverse from Zhongshan to Dome A.

We selected 142 seismic events for analysis; for each event, the epicentral distance was in the range of  $55^{\circ}$ – $85^{\circ}$ , the magnitude was greater than 5.5, and the signal-to-noise ratio was high; the distribution of epicentres is shown in Figure 3. The selected seismic data were then rotated from a vertical–north–east (ZNE) to a vertical–radial–transverse (ZRT) coordinate system. Finally, the S-wave receiver functions were obtained by an iterative time–domain deconvolution ([Ligorriá and Ammon, 1999](#)) based on the radial and vertical components. As in the case of regular P-wave receiver functions, we inverted the amplitude and time axes of the S-wave receiver functions so that the converted wave phases (Smp or Sp) and delay times were positive.

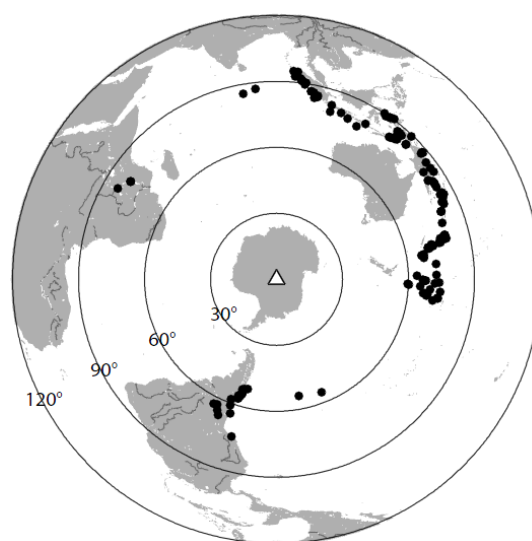


Figure 3. Locations of analysed seismic events (black dots)

Figure 4 shows the S-wave receiver functions from stations EAGLE and DOMEA, arranged in sequential order based on back-azimuth values. The Sp phase (peak labelled by Sp in Figure 4) of the converted wave at the Moho is clearly shown, regardless of whether the receiver functions are viewed individually or after stacking.

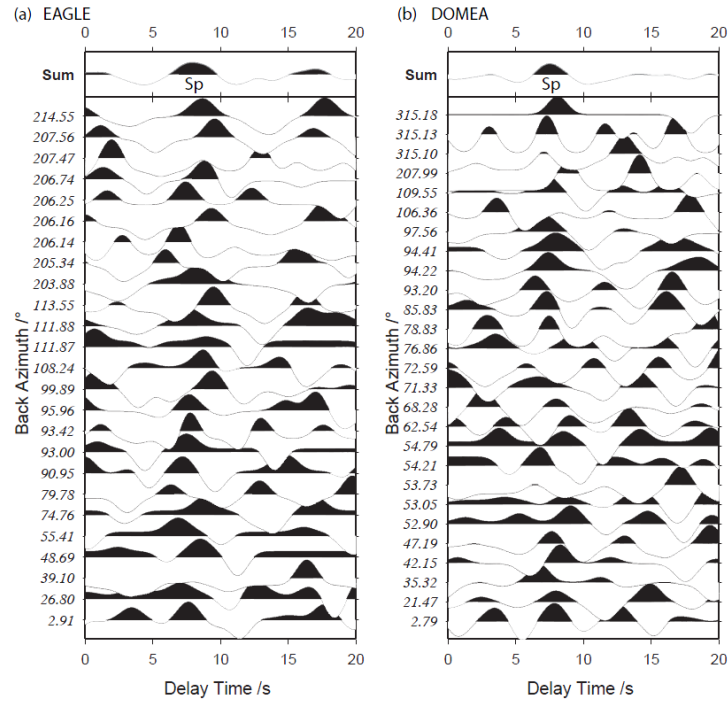


Figure 4. S-wave receiver functions for the EAGLE (a) and DOMEA (b) stations. The stacked receiver function for each station is shown at the top of each diagram.

To increase the signal-to-noise ratio, the stacked receiver function for each station was used in the inversion process to obtain the crustal thickness beneath the station. The stacked receiver functions of all stations are shown in order from low to high latitude (i.e., from stations ZHSH to DOMEA) in Figure 5. The reliability of the stacked receiver function at a given station increases in proportion to the number of receiver functions.

Figure 5 shows that the delay time of the Sp phase progressively increases between stations ZHSH and EAGLE, progressively decreases between stations EAGLE and CHNA, and increases again at Kunlun (station DOMEA). The time-delay variation indicates that the crustal thickness gradually increases between stations ZHSH and EAGLE, then gradually decreases between stations EAGLE and CHNA, and finally increases again at station DOMEA.

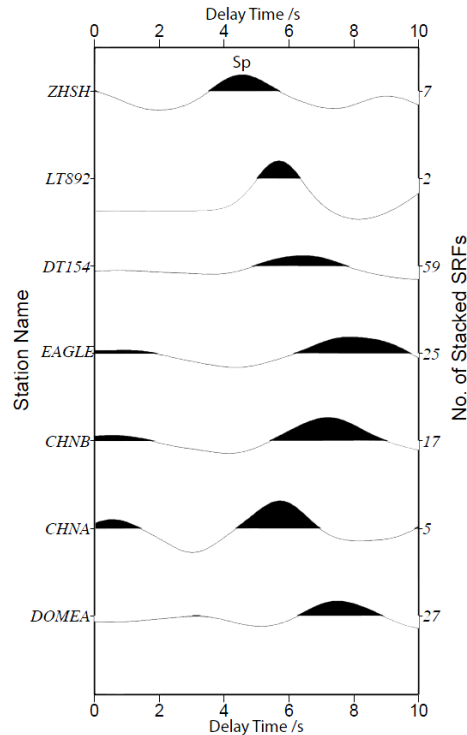


Figure 5. Stacked S-wave receiver functions for the seven Chinese seismic stations, ordered from low (top) to high (bottom) latitudes. The horizontal axis represents the delay time of the Sp phase relative to the direct S-wave. The names of the stations are marked on the left vertical axis, and the numbers of S-wave receiver functions used at each station is marked on the right vertical axis.

### 2.3 Inversion for crustal thickness

We used an enumerate (or called grid search) method to jointly invert surface wave dispersions and Sp delay times to obtain crustal thicknesses, similar to the method used by Hansen et al. (2009). The first step in the inversion is the forward calculation of the Sp delay times and the Rayleigh-wave group-velocity dispersions for all possible models, including those for crustal thickness and average velocities in the crust. For each station, the calculated values were then compared with observed values, thus yielding the misfit of the synthetic model at each station. Models with a relatively small misfit for surface wave dispersion and Sp delay time were selected as acceptable. The average crustal thickness determined by all acceptable models was taken as the final crustal thickness beneath the station.

The above strategy, which is actually a multiple-objective inversion, involves the simultaneous fitting of the surface wave dispersion and the Sp delay time (An and Assumpção, 2004). In a multi-objective inversion, any model that fits an observation well is usually considered a good model. For this reason, we took the weighted sum of all misfits as

a comprehensive misfit value, and used this value to evaluate each model; this method is unlike the method used by Hansen et al. (2009), in which a model is selected according to two separated misfit values and a accepted model must simultaneously fit all observations well. When the weighted sum of all misfits is used, an optimum fit using any of the observations is taken as a good model, even if the model fit to some observations is relatively poor. However, a model that fits all observations at acceptable levels, but which does not fit any observation well, may be discarded.

During the process of forward calculation, all models are parameterized in terms of four layers: an ice layer, upper and lower crustal layers, and an upper mantle half-space. The thicknesses of the upper and lower crust are assumed to be equal. The thickness of the ice layer beneath each station remains constant, and, except for station ZHSH which is installed on rock, was obtained from the Bedmap2 model (Fretwell et al., 2013), which contains the latest results on ice thickness determined by international explorations since the 4<sup>th</sup> IPY. The S-wave velocities in the ice layer and the upper mantle were fixed at 1.9 and 4.5 km/s, respectively. Crustal thicknesses were sampled between the depths of 30 and 65 km with an interval of 1 km. The S-wave velocities of the upper and lower crust were in the range of 3.4–3.9 km/s at an interval of 0.05 km/s. The Poisson ratios for the ice layer, crust, and mantle in all models were 0.33, 0.25, and 0.28, respectively.

The Sp delay times were derived from the S-wave receiver functions of this study, whereas the Rayleigh wave group velocities (with periods of 10–200 s) beneath the seven seismic stations (Figure 6) were obtained from surface-wave tomography of the Antarctic plate (An et al., 2013). The misfits for all possible models for DOMEA, for surface wave dispersions (horizontal axis) and Sp delay times (vertical axis), are shown with black dots in Figure 7. In the figure, red dots show acceptable models, as determined by the weighted sum of the misfits for the surface waves and Sp delay time.

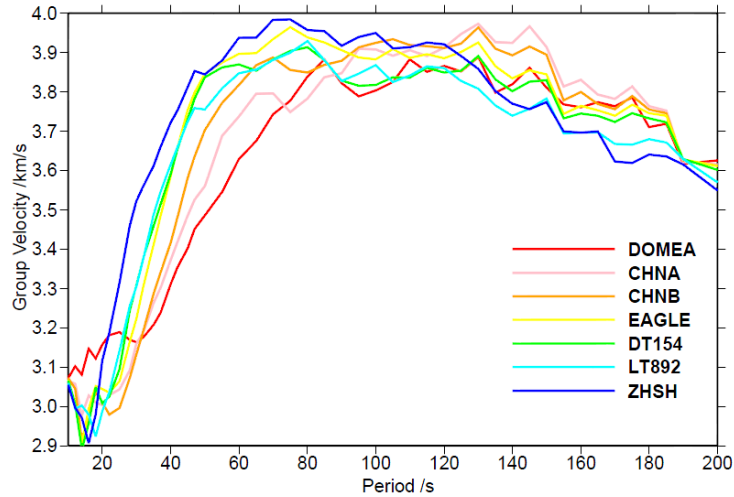


Figure 6. Rayleigh wave group velocities recorded beneath the seven seismic stations

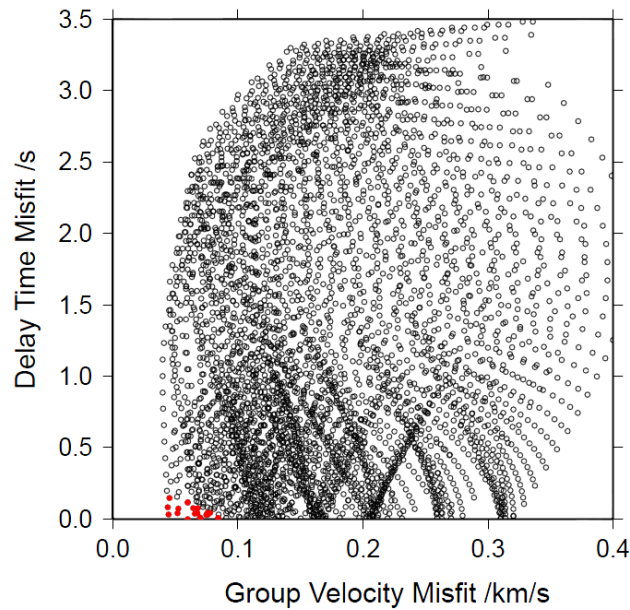


Figure 7. Misfits of surface-wave group velocities and  $S_p$  delay times for all possible models for station DOMEA. Red dots indicate acceptable models.

### 3. Results

The average of all acceptable models for each station (e.g., their misfits for DOMEA are indicated by red dots in Figure 7) was used to represent the S-wave velocity profiles and the crustal thickness beneath each station. The average S-wave velocity profiles beneath each station are shown in Figure 8, and the crustal thickness beneath each station is shown in

Figure 9 and listed in Table 1. The thickness of the ice layer under each station, shown in Figure 8 and Table 1 (data not given for station ZHSH, as it is located on bedrock), was obtained from Bedmap2. The crustal thickness results (Figure 9 and Table 1) indicate that the crust is thinnest at the continental margin beneath station ZHSH (thickness, ~38 km), and thickest beneath the highest point of Antarctica at station DOMEA (~62 km).

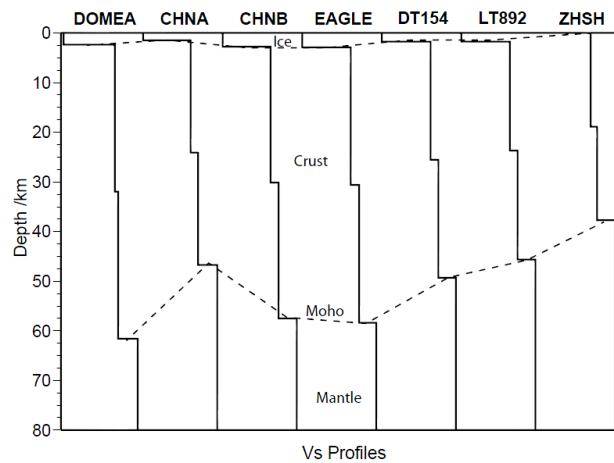


Figure 8. S-wave velocity profiles beneath the seismic stations along the traverse from station ZHSH to DOMEA.

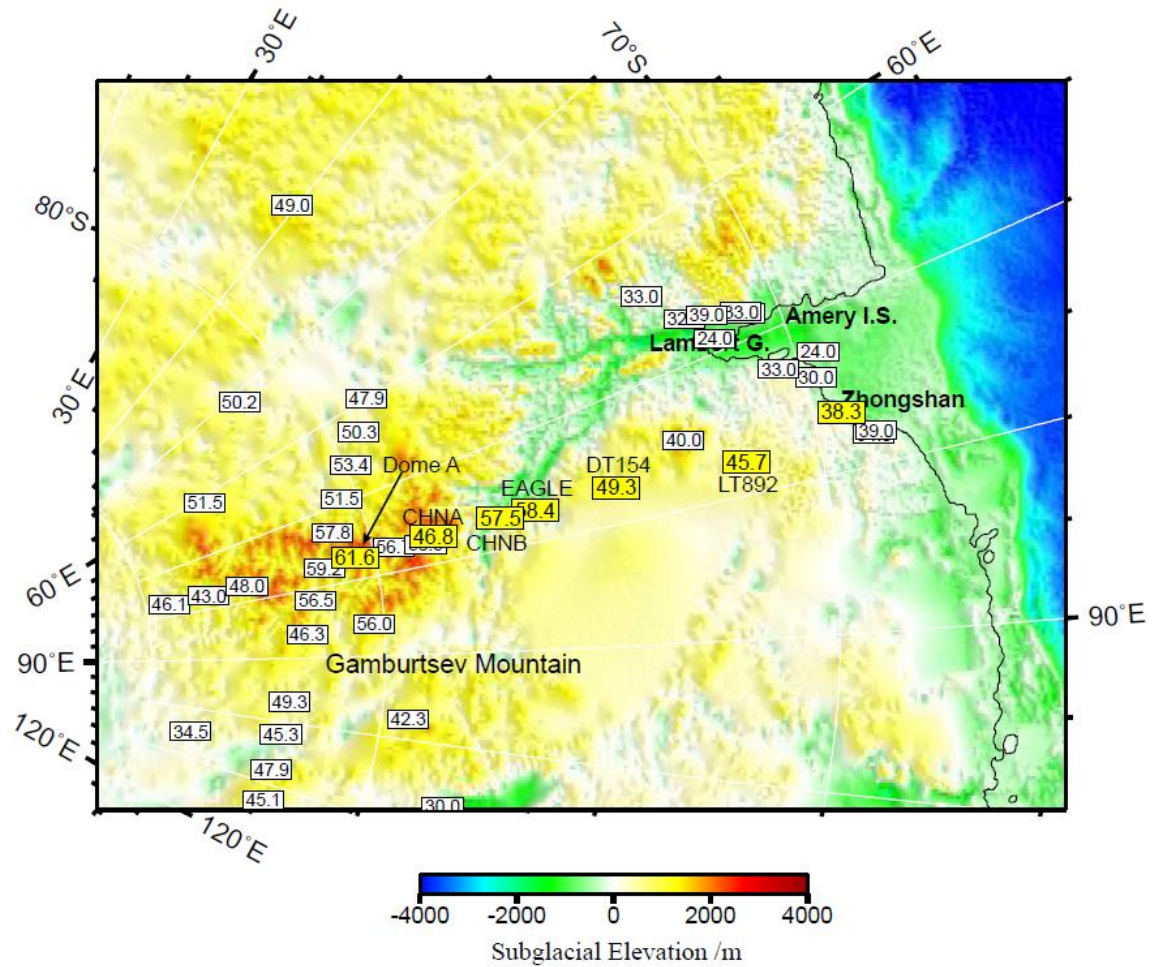


Figure 9. Elevation map showing the distribution of crustal thickness in the vicinity of the Gamburtsev Subglacial Mountains and Lambert Glacier. Crustal thickness beneath each of the Chinese stations is labelled in yellow; other crustal thickness values are the same as those shown in Figure 1.

**Table 1. Crustal thickness and ice thickness beneath the Chinese stations.**

Station	Lat. (°)	Long. (°)	Elev. (m)	Ice layer thickness (km)	Crustal thickness (km)
ZHSH	-69.3747	76.3727	26	0	38.3
LT892	-71.6708	77.7670	2230	1.807	45.7
DT154	-74.5824	77.0257	2718	1.805	49.3
EAGLE	-76.4154	77.0448	2833	2.864	58.4
CHNB	-77.1744	76.9760	2960	2.808	57.5
CHNA	-78.6770	77.0130	3530	1.528	46.8
DOMEA	-80.4220	77.1047	4091	2.446	61.6

Along the CHINARE traverse between stations ZHSH and CHNB, the crustal thickness gradually increases from 38 km at station ZHSH to 58 km at station CHNB, and then

decreases to 47 km at station CHNA. This trend indicates that the structure of the crust between stations ZHSH and CHNB is relatively homogenous, whereas the crust beneath the region close to CHNA is more heterogeneous. The variations in subglacial topography shown in Figure 9 indicate that the area between stations ZHSH and CHNB comprises a single geomorphic unit, whereas station CHNA is located above another geomorphic unit. Thus, the changes in crustal thickness correspond to topographic variations, indicating that crustal thickness values should be reliable, and that the results obtain here reflect the structure of the crust beneath the stations.

Kunlun Station (station DOMEA) is located at the highest point on Antarctica, which is also the region of the thickest crust thus far measured on the continent (62 km; see Figure 9 and Table 1) ([An et al., 2013](#)). The craton of East Antarctica is fundamentally stable. However, the crustal thickness beneath station DOMEA is much greater than that of other continental cratons, and is generally similar to the crustal thickness in subduction and collision orogens, such as the Andes and the Tibetan Plateau, respectively. Thus, it can be deduced that the thickening of the crust beneath DOMEA may have been caused by subduction or collision processes. Because East Antarctica has been stable for long periods of time during the Phanerozoic, the crust beneath station DOMEA has not undergone obvious changes since its formation. For this reason, the thickened crust in this region must represent an ancient orogenic crustal root.

The crustal thickness beneath station CHNA (46.8 km) is less than that beneath station DOMEA, which is located approximately 200 km away, and is also less than that beneath US seismic station P124 (57.5 km; see Figure 9), which is located only 30 km away. These patterns of crustal thickness may simply reflect the short duration of observations at station CHNA. However, if the location of station DOMEA had been part of a collisional orogeny in the past, then relatively large horizontal variations in crustal structure should appear in the surrounding region. In this case, it is possible that substantive variations in crustal structure may occur over distances of several tens of kilometres. Moreover, station CHNA is close to topographic lows in the bedrock surface (between stations CHNA and CHNB; see Figure 9), indicating that the crust beneath the topographic lows is different than that beneath other regions. Therefore, the crustal thicknesses derived above should represent reliable results, and

should provide information on structures beneath the stations. A thin crust beneath CHNA indicates that the crust beneath the GSM underwent relatively large lateral changes and complex tectonism during its formation.

Figure 9 and Table 1 show good correlations between the trends in lateral variations of crustal thickness and the thickness of the ice layer beneath the respective stations. At station ZHSH, where the crust is thinnest, the thickness of the ice layer approaches zero. On the other hand, at station DOMEA, where the crust is thickest, the ice layer is 2 km thick. The crust and the ice layer beneath station CHNA, located between ZHSH and DOMEA, are both relatively thinner.

#### **4. Conclusions**

Since the 4th IPY in 2007/08, and as part of the international collaborative project GAMSEIS and China's PANDA project, the CHINARE team has installed eight cold-mode very broadband seismic stations along the traverse between Zhongshan and Kunlun Stations (Dome A), and has obtained seismic data on deep structures beneath the traverse. Seismic observations from seven of the stations were sufficient to determine the crustal thickness beneath each station.

The crustal thickness beneath Zhongshan is 38 km. From Zhongshan station, crustal thickness increases to 58 km beneath station CHNB, decreases to 47 km beneath station CHNA, and increases dramatically to 62 km beneath Kunlun Station (Dome A). The crust beneath Dome A is the thickest known crust on the entire Antarctic continent. The pattern of crustal thickness changes along the traverse indicates that crustal structures between Zhongshan and station CHNB are relatively uniform, but that greater structural heterogeneity is present between station CHNB and Kunlun Station; structural heterogeneities are especially pronounced beneath station CHNA. Changes in crustal structure and thickness are reflected to a certain degree in the bedrock surface topography. As expected, a significant correlation exists between crustal thickness and subglacial topography in the region.

The craton of East Antarctica is stable for a long time. However, the crustal thickness of 62 km beneath Dome A, as determined in this study, is much greater than that of other continental cratons, and is very similar to that of subduction or collision zone orogens, such

as the Andes and Tibetan Plateau, respectively. Thus, it can be deduced that crustal thickening beneath Kunlun Station represents the ancient orogenic crustal roots of a collision or subduction orogen. The crust beneath station CHNA is thinner than that beneath Kunlun Station, which is located approximately 200 km away, and is significantly thinner than that beneath station P124 of GAMSEIS, located only 30 km away. These results indicate relatively large lateral changes in the thickness and characteristics of the crust in the GSM region, and that the crust in the region has undergone periods of tectonism and a complex formation history.

### **Acknowledgments**

Our work was supported by the National Natural Science Foundation of China (grant No. NSFC-40874021), Chinese Polar Environment Comprehensive Investigation & Assessment Programmes (grant No. CHINARE2013-04-02), the Chinese Program of Antarctic Nova Disciplines Aspects in the International Polar Year. All field work was conducted by the 24<sup>th</sup>–29<sup>th</sup> Chinese National Antarctic Research Expeditions during 2007–2013, and the fieldwork at the seismic stations during the 24<sup>th</sup> expedition (2007/08) was conducted by Dr. Xiao Cheng. We are grateful for the logistical support of the Antarctic Administration of China and all members of the Chinese inland icecap expeditions. All figures are generated using the Generic Mapping Tools (GMT) ([Wessel and Smith, 1991](#)).

### **References**

- An, M., Assumpção, M.S., 2004. Multi-Objective Inversion of Surface Waves and Receiver Functions by Competent Genetic Algorithm Applied to the Crustal Structure of the Paraná Basin, SE Brazil. *Geophys. Res. Lett.*, 31(5), L05615. doi:10.1029/2003GL019179.
- An, M., Wiens, D., Zhao, Y., Feng, M., Nyblade, A., Kanao, M., Li, Y., Maggi, A., Lévêque, J., 2013. 3D Lithosphere Structure of the Antarctic Plate and its Geodynamical Implications on the Plate Evolution, IAHS/IAPSO/IASPEI Joint Assembly 2013, Gothenburg, Sweden.
- Baranov, A., Morelli, A., 2013. The Moho depth map of the Antarctica region. *Tectonophysics*, (0). <http://dx.doi.org/10.1016/j.tecto.2012.12.023>.
- Bayer, B., Geissler, W.H., Eckstaller, A., Jokat, W., 2009. Seismic imaging of the crust beneath Dronning Maud Land, East Antarctica. *Geophysical Journal International*, 178(2), 860-876. 10.1111/j.1365-246X.2009.04196.x.
- Fretwell, P., Pritchard, H.D., Vaughan, D.G., Bamber, J.L., Barrand, N.E., Bell, R., Bianchi, C., Bingham, R.G.,

- Blankenship, D.D., Casassa, G., Catania, G., Callens, D., Conway, H., Cook, A.J., Corr, H.F.J., Damaske, D., Damm, V., Ferraccioli, F., Forsberg, R., Fujita, S., Gim, Y., Gogineni, P., Griggs, J.A., Hindmarsh, R.C.A., Holmlund, P., Holt, J.W., Jacobel, R.W., Jenkins, A., Jokat, W., Jordan, T., King, E.C., Kohler, J., Krabill, W., Riger-Kusk, M., Langley, K.A., Leitchenkov, G., Leuschen, C., Luyendyk, B.P., Matsuoka, K., Mouginot, J., Nitsche, F.O., Nogi, Y., Nost, O.A., Popov, S.V., Rignot, E., Rippin, D.M., Rivera, A., Roberts, J., Ross, N., Siegert, M.J., Smith, A.M., Steinhage, D., Studinger, M., Sun, B., Tinto, B.K., Welch, B.C., Wilson, D., Young, D.A., Xiangbin, C., Zirizzotti, A., 2013. Bedmap2: improved ice bed, surface and thickness datasets for Antarctica. *The Cryosphere*, 7(1), 375-393. doi:10.5194/tc-7-375-2013.
- Hansen, S.E., Julià, J., Nyblade, A.A., Pyle, M.L., Wiens, D.A., Anandkrishnan, S., 2009. Using S wave receiver functions to estimate crustal structure beneath ice sheets: An application to the Transantarctic Mountains and East Antarctic craton. *Geochem. Geophys. Geosyst.*, 10(8), Q08014. 10.1029/2009gc002576.
- Hansen, S.E., Nyblade, A.A., Heeszel, D.S., Wiens, D.A., Shore, P., Kanao, M., 2010. Crustal structure of the Gamburtsev Mountains, East Antarctica, from S-wave receiver functions and Rayleigh wave phase velocities. *Earth and Planetary Science Letters*, 300(3-4), 395-401. 10.1016/j.epsl.2010.10.022.
- Harrowfield, M., Holdgate, G.R., Wilson, C.J.L., McLoughlin, S., 2005. Tectonic significance of the Lambert graben, East Antarctica: Reconstructing the Gondwanan rift. *Geology*, 33(3), 197-200. 10.1130/g21081.1.
- Langston, C.A., 1979. Structure under Mount Rainier, Washington, inferred from teleseismic body waves. *J. Geophys. Res.*, 84(B9), 4749-4762.
- Ligorri, J.P., Ammon, C.J., 1999. Iterative deconvolution and receiver-function estimation. *Bull. Seism. Soc. Amer.*, 89, 1395-1400.
- Mohorovičić, A., 1910. Potres od 8. X. 1909 (in in Croatian). *Godišnje izvješće Zagrebačkog meteorološkog opservatorija za godinu 1909*, (9/4), 1-56.
- Phillips, G., Läufer, A.L., 2009. Brittle deformation relating to the Carboniferous–Cretaceous evolution of the Lambert Graben, East Antarctica: A precursor for Cenozoic relief development in an intraplate and glaciated region. *Tectonophysics*, 471(3–4), 216-224. 10.1016/j.tecto.2009.02.012.
- Wessel, P., Smith, W.H.F., 1991. Free software helps map and display data. *EOS Trans. AGU*, 72, 441. doi:10.1029/90EO00319.
- Winberry, J.P., Anandkrishnan, S., 2004. Crustal structure of the West Antarctic rift system and Marie Byrd Land hotspot. *Geology*, 32(11), 977-980. 10.1130/g20768.1.